Galindo, J.; Climent, H.; De La Morena, J.; González-Domínguez, D.; Guilain, S.; Besancon, T. (2021). Experimental and modeling analysis on the optimization of combined VVT and EGR strategies in turbocharged direct-injection gasoline engines with VNT. Proceedings of the Institution of Mechanical Engineers Part D Journal of Automobile Engineering. 235(10-11):2843-2856. https://doi.org/10.1177/09544070211004502

Experimental and modeling analysis on the optimization of combined VVT and EGR strategies in turbocharged direct-injection gasoline engines with VNT

José Galindo[a], Héctor Climent[a], Joaquín de la Morena[a], David González-Domínguez[a,*] Stéphane Guilain[b], Thomas Besançon[b]

[a] CMT Motores Térmicos, Universitat Politècnica de València, Spain
[b] Renault SAS, France.

*Corresponding author: dagondo1@mot.upv.es. Telephone: (+34) 96 387 76 50. Postal address: CMT-Motores Térmicos. Universitat Politècnica de València. Camino de Vera s/n. 46022. Valencia. Spain.

Acknowledgements: the authors would like to thank Vicente Esteve, Rafael Pitarch and Irina Jimenez for their invaluable work during the experimental campaign.

Funding: this research work received no external funding.

Conflicts of interest: the authors declare no conflict of interest.

Abstract

The combination of a growing number of complex technologies in internal combustion engines (ICE) is commonplace, due to the need of complying with the tight pollutant regulations and achieving high efficiencies. Hence the work of calibration engineers is led by a constant increase in degrees of freedom in ICE design. In this research work, a wide analysis on the optimization of combined variable valve timing (VVT) and exhaust gases recirculation (EGR) strategies is developed, in order to reduce fuel consumption in a EURO 6 1.3l 4-stroke 4-cylinder, gasoline, turbocharged, direct-injection engine, also equipped with a variable nozzle turbine (VNT). For that purpose, a methodology which combines 1D engine simulations with limited experimental work was applied. First, the data from 25 experimental tests distributed into three steady engine operating conditions was used to calibrate a 1D model. Then, modeling parametric studies were performed to optimize VVT and EGR parameters. A total of 150 cases were simulated for each operating point, in which VVT settings and EGR rate were varied at iso-air mass flow and iso-intake manifold temperature. The optimization was based on finding the configuration of VVT and EGR systems which maximizes the indicated efficiency. All different cases modeled were also evaluated in terms of pumping and heat losses. Moreover, a deep assessment of instantaneous pressure traces and mass flows in intake and exhaust valves was given, to provide insights about the optimization procedure. Finally, the findings obtained by simulation were compared with the results from a design of experiments (DOE) composed of more than 300 tests, and the impact on engine fuel consumption was analyzed.

Acronyms

AMF	Air mass flow
ANN	Artificial neural network
ATDC	After top dead center
BDC	Bottom dead center
BMEP	Brake mean effective pressure
BTDC	Before top dead center
CA50	Crank-angle degree at 50% heat release
CAD	Crank-angle degrees
C_d	Discharge coefficient
COV	Coefficient of variation
DOE	Design of experiments
EATS	Exhaust aftertreatment system
ECU	Engine control unit
EGR	Exhaust gases recirculation
EVC	Exhaust valve closing
FM	Friction multiplier
FMEP	Friction mean effective pressure
FWC	Four-way catalyst
GPF	Gasoline particulate filter
GTDI	Gasoline turbocharged direct injection
HTM	Heat transfer multiplier
ICE	Internal combustion engines
IMEP	Indicated mean effective pressure
IVO	Intake valve opening
LP	Low pressure
MAPE	Mean absolute percentage error
MPE	Mean percentage error
PI	Proportional-integral
PMEP	Pumping mean effective pressure
RGF	Residual gas fraction
TOC1090	Combustion duration in crank-angle degrees from 10% to 90% heat release
TWC	Three-way catalyst
VNT	Variable nozzle turbine
VVT	Variable valve timing
WCAC	Water charge air cooler

1. Introduction

Fuel economy is a major concern in engine research. Spark ignited (SI) engines have gained attention in the automotive market in Europe in the last decade, since the complexity and costs of after-treatment devices in compression ignition (CI) engines have increased with the tight pollutant emission regulations. Moreover, great research and development efforts have been carried out to design more efficient SI engines in terms of

fuel consumption, which is directly related with CO_2 emissions, while the other exhaust emissions are usually under control by means of the well-known three-way catalyst technology and, eventually, gasoline particulate filters.

An attractive strategy to reduce fuel consumption on SI engines consists of turbocharged engines with direct injection fuel systems, where the high engine thermal efficiency zone in the engine map is enlarged and shifted from high to medium engine loads [1, 2]. This so-called downsizing SI engine technology along with direct injection reduces the fuel consumption by decreasing the pumping losses and increasing the compression ratio [3, 4]. The use of a turbocharger in a SI engine is not exempt from issues, mainly related to gas temperature limitations at the turbine inlet, which usually occurs at high load engine operation. Traditionally, the turbine protection function can be achieved by injecting more fuel than the stoichiometric value, in order to reduce the combustion temperature. This strategy, however, does not fulfill the fuel reduction objective that is widely sought.

Other interesting strategies are being employed to improve fuel economy in the SI research area, such as the introduction of cooled exhaust gas recirculation (EGR) [5], variable valve timing (VVT) system [6], deactivation of cylinders [7] and intake port injection of water [8]. Focusing on the EGR technology, it reduces the knocking tendency [9, 10], the pumping losses, the exhaust gas temperature and the heat losses through the cylinder walls [11, 12]. It has been reported in the literature that introducing cooled EGR at high loads avoids the need of engine operation in fuel enriched conditions to control the exhaust gas temperature [13, 14].

In the present research work, the interaction between VVT and EGR strategies in gasoline ICE was studied, because of their capability to enhance the engine performance. Another good motivation to perform this study is the increase in degrees of freedom in calibration tasks, due to the complexity of modern SI engines where a large number of input variables (such as spark timing, intake and exhaust valve openings, EGR rate, throttle and variable nozzle turbine positions) must be optimized by calibration teams.

For these reasons, the paper is focused on analyzing the optimization process of combined VVT and EGR strategies to minimize fuel consumption in a gasoline, turbocharged, direct-injection (GTDI) engine, also equipped with a variable nozzle turbine (VNT). To this end, a method which combines 1D engine simulations with limited experimental work was applied. It is widely accepted that engine testing in combination with accurate models is a key approach to achieve productive results [15, 16]. Besides, there are several advantages of using models compared to experimental methods when solving a problem [17, 18], for instance, computer simulation costs are generally lower than those derived from experimental testing.

However, the 1D model of the engine operating with cooled EGR requires a previous calibration. Twenty-five experimental tests, distributed into three steady-state engine running conditions, were performed to adjust the 1D model. The experimental facility consists of a EURO 6 GTDI engine equipped with a custom low pressure EGR loop, which was designed to provide the flexibility needed to carry out the reported research

activities. Regarding the calibration of the 1D model, it is based on the procedure described for an analogous GTDI engine operating without EGR in a former study [19].

The paper is structured as follows. Section 2 is devoted to the experimental setup, engine and instrumentation descriptions. The model details are explained in Section 3. Section 4 describes the used methodology that combines experimental and modeling tasks. The results and consequent analysis are found in Section 5. Finally, the main conclusions are presented in Section 6.

2. Experimental setup

For the present work, a EURO 6 SI GTDI 1.3l 4-stroke 4-cylinder engine was employed, whose principal attributes are summarized in Table 1. The engine also includes four-way catalyst (FWC) and VVT technologies. The FWC aftertreatment system combines the functionality of a conventional three-way catalyst (TWC) with a gasoline particulate filter (GPF), removing all four pollutants with just one component. Concerning the VVT system, it enables to advance or delay the camshaft timing in a range of forty degrees for both intake and exhaust sides, while keeping constant the valve lift and opening duration. The turbocharger is equipped with a variable nozzle turbine (VNT) as well. In addition, a low pressure (LP) EGR loop was appended to the base engine. It is basically composed of a T-connection duct to extract exhaust gases downstream the aftertreatment system, a water-to-air intercooler and one EGR valve located downstream. In order to allow higher EGR rates, a choke valve was also added in the intake air-path, just upstream the EGR junction. A diagram of the engine layout and flow connections is attached in Figure 1.

Table 1: Engine's features

Type	Gasoline Euro 6
Displacement	1300 cc
Compression ratio	10:1
Number of cylinders	4
Type of injection	Direct injection
Camshaft system	Variable Valve Timing
Number of valves per cylinder (intake/exhaust)	2/2
Turbocharger	VNT technology
Aftertreatment system	Four-way catalyst

The engine was fully instrumented and installed in a dynamic test bench, which was controlled with the AVL PUMA software. It allows regulating the engine speed and torque through the AVL AFA 200/4-8EU dynamometric brake. The main cycle-averaged pressure and temperature values, air and fuel mass flows, turbocharger speed and exhaust emissions were also recorded by means of the AVL PUMA software. The location of the cycle-averaged pressure (Kistler 4260A piezoresistive type transmitters) and temperature (3mm K-type thermocouples) sensors can be found in Figure 1. The turbocharger speed

and the air and fuel mass flows were acquired with the systems MICRO-EPSILON DZ140, AVL FLOWSONIX and AVL 733S, respectively. Besides, a HORIBA MEXA-ONE system was installed to register exhaust gas emissions measurements (NOx, HC, CO, CO_2 and O_2). The EGR rate was estimated through intake and exhaust CO_2 concentrations as follows [20]:

$$\text{EGR}\,[\%] = \frac{[CO_2]_{\text{intake}} - [CO_2]_{\text{ambient}}}{[CO_2]_{\text{exhaust}} - [CO_2]_{\text{ambient}}} \cdot 100 \quad (1)$$

where the intake ($[CO_2]_{\text{intake}}$) and exhaust ($[CO_2]_{\text{exhaust}}$) mole fractions of CO_2 were measured at the intake manifold and aftertreatment outlet, respectively. The $[CO_2]_{\text{ambient}}$ represents the ambient mole fraction of CO_2.

In addition, the instantaneous pressures in both manifolds and in the four cylinders were measured, by using two Kistler 601CAA piezoelectric type sensors for the manifolds and four AVL Z133 spark plugs with integrated pressure sensors for the cylinders. These six instantaneous pressure signals were registered with a sampling of 0.2 crank-angle degrees, through the PXI 6123 and PXI 6251 acquisition modules programmed with Labview by National Instruments TM [21, 22]. The original engine control unit (ECU), designed for the base engine without EGR, was partially bypassed with an ETAS ES910 system to enable any variations on the VVT system, main throttle position, spark timing, and injected fuel. Finally, the VNT position, EGR valve and intake throttle (Figure 1) were directly managed in open-loop configuration independently from the ECU, by means of the NI 9759 and PXI 7813R control modules [21, 22].

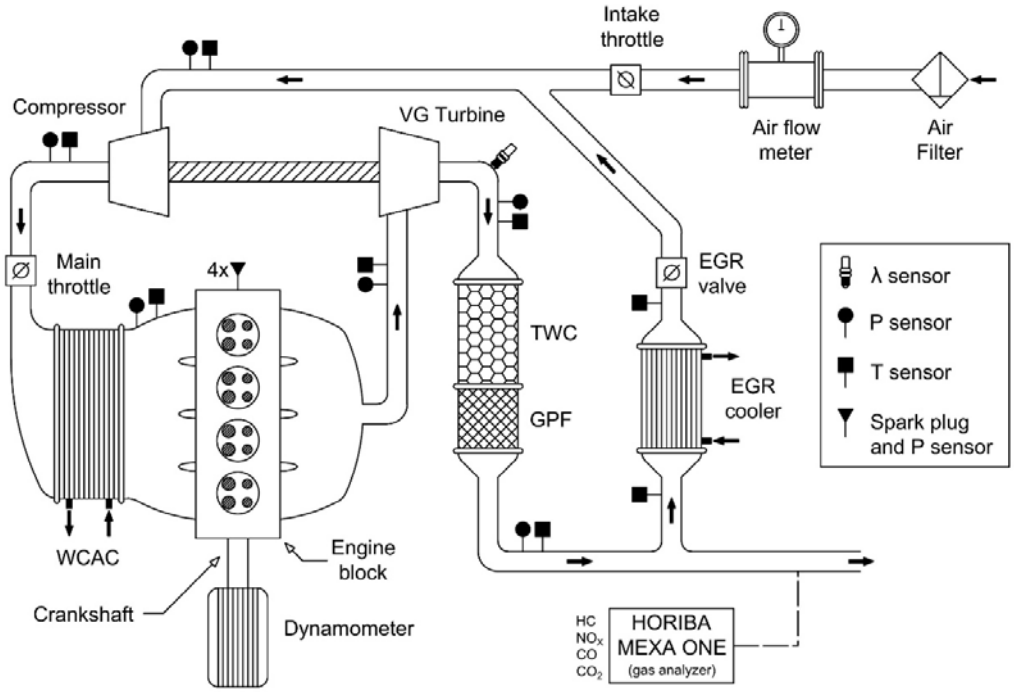

Figure 1: Schematic engine layout.

3. Modeling tools

The model used in this study is built on a 1D model of an analogous GTDI engine, also with VVT and VNT technologies, but without an EGR system. This base model was developed by means of the market-leading software GT-Power and calibrated according to the procedure described by Serrano et al [19]. In summary, this procedure is mostly characterized by isolating the different engine parts, decoupling the turbocharger, and using proportional-integral (PI) controls to achieve fitting parameters. It also includes the determination of empirical correlations to estimate heat losses and pressure drops in engine systems, and the training of an artificial neural network (ANN) to predict the Wiebe parameters and so to reproduce the combustion process [19]. After that, in order to complete the model calibration, the cycle-averaged variables (the most critical values of pressure and temperature and the air mass flow) and crank-angle resolved pressure signals (in the cylinders and both manifolds) are checked to validate the ANN and correlations performance.

However, those empirical equations and ANN already obtained for the base model could not be reused, even though both engines have the same block. This is because some significant modifications were introduced into the current engine. As stated before, an LP-EGR loop was added and, in consequence, the exhaust line had to be adapted too. Moreover, the exhaust manifold geometry was modified to enable the addition of a high pressure EGR loop, which is not used in the current study. Finally, the intake manifold geometry was updated including an integrated water charge air cooler (WCAC).

Therefore, a GT-Power ICE 1D model was employed for this research work. The model was restructured according to the above-mentioned engine modifications and readjusted by following the same calibration procedure described in [19], but with some slight differences, as will be stated in the Methodology section.

4. Methodology

The present study proposes an alternative methodology to the conventional design of experiments (DOE). This method is mainly based on 1D-modeling simulations supported with only the experimental work required to adjust the engine model. Thus, it aims to reduce workload and costs in the engine test bench. In addition, it must be remarked that the use of modeling techniques has a second advantage. It usually eases the understanding of the results, since it allows analyzing some variables which cannot be experimentally obtained, like instantaneous mass flows in the intake and exhaust valves or in-cylinder residual gas fraction (RGF). The entire methodology is explained in detail below.

First, an experimental campaign, composed of a total of twenty-five tests, was performed for the model calibration. The most relevant features of these experiments are summarized in Table 2, where the number of points tested and the operating ranges of the main cycle-averaged variables (in square brackets) for each working point (defined by the engine speed and load) are shown. As noticed in Table 2, three steady engine running conditions were analyzed in this study: 6 bar BMEP at 1500 and 2000 rpm, and 12 bar BMEP at 3000 rpm. All three working points were tested for several EGR rates with different VVT

settings, in order to adjust the model for a wide range of these variables. Regarding the VNT, it was used to reach the desired load at 3000 rpm for EGR rates higher than around 15%. Moreover, the spark timing was set for each test by considering that the optimum combustion start generally leads to a value of CA50 (crank-angle degree at 50% heat release) from 5 to 10 CAD (crank-angle degrees) ATDC (after top dead center), as stated in [23]. For that purpose, a real-time apparent heat release rate estimation from the in-cylinder pressure signals was used in the engine test rig, as described in [22].

Table 2: Summary of the experimental campaign (in the square brackets, the operating ranges of the different variables)

Variable	**1500x6 tests**	**2000x6 tests**	**3000x12 tests**
Engine speed (rpm)	1500	2000	3000
BMEP (bar)	6	6	12
Number of points tested	8	9	8
Air mass flow (kg/h)	[32, 36]	[44, 48]	[120, 125]
EGR (%)	[0, 22]	[0, 23]	[0, 20]
Intake manifold pressure (bar)	[0.70, 0.90]	[0.65, 0.85]	[1.05, 1.25]
Intake manifold temperature (ºC)	[26, 33]	[30, 33]	[26, 29]
Exhaust manifold pressure (bar)	[1.05, 1.06]	[1.08, 1.09]	[1.27, 1.34]
Spark timing (CAD BTDC)	[10, 25]	[10, 30]	[7, 21]

Once the experiments were done, a calibration procedure was needed to accomplish a predictive and accurate engine 1D model. It was carried out in three stages: obtention of fitting parameters, model validation and determination of empirical correlations. In the first stage, the twenty-five engine tests (Table 2) were simulated to obtain fitting parameters (heat transfer multipliers [HTM], friction multipliers [FM] or discharge coefficients [C_d], among others) which adjust phenomena of heat transfer and pressure drop in engine lines and volumes. For these simulations, the model was set in 'fitting mode', which mainly consists of two techniques: the use of PI controllers to modify the fitting parameters, and the turbocharger decoupling by unlinking compressor and turbine powers. The latter allows controlling the intake and exhaust manifold conditions at the same time. Both the configuration of PI controllers and the turbocharger decoupling maneuver were described in detail by Serrano et al [19]. Besides, the experimental EGR rate was achieved for all the simulations, by means of a closed-loop controller which regulates the positions of the intake throttle and EGR valve (Figure 1). Regarding the combustion process, it was modeled through the Wiebe function [24], whose parameters were estimated from the cumulative apparent heat release, as explained in [22]. Furthermore, the ambient conditions, engine speed, air-to-fuel ratio, friction mean effective pressure (FMEP) and VVT settings of the twenty-five cases were directly imposed into the model.

After that, a validation process was required to achieve reliable empirical correlations, and so to ensure the high-quality of the model calibration. To this end, the modeled and experimental values of the cycle-averaged air mass flow (AMF), indicated mean effective

pressure (IMEP) and instantaneous pressure traces were compared for the same twenty-five tests (Table 2). In addition, an error threshold of 5% was considered for both AMF and IMEP variables. This way, the fitting parameters of each case were only used as inputs for the empirical correlations, if its corresponding AMF and IMEP relative errors were lower than 5%. Regarding the rest of cycle-averaged variables (such as the pressure and temperature values at compressor inlet and outlet, turbine inlet and outlet and intake manifold, and the EGR rate), they were perfectly reproduced (errors of around 0%) via modeling, because the PI controllers were activated during the simulations.

To complete the calibration procedure, the last stage is the determination of empirical correlations with the fitting parameters from the twenty-five validated simulations. Four equations were introduced into the model to compute the values of EGR line HTM, exhaust manifold HTM, orifice C_d in exhaust line and FMEP. Regarding the combustion modeling, another equation was defined to estimate the TOC1090 (combustion duration in crank-angle degrees from 10% to 90% heat release), as a function of the modeled in-cylinder gas temperature and residual gas fraction at intake valve closing, and engine speed [25]. The effect of the combustion phasing on TOC1090 was neglected in this case, given that a constant CA50 value of 7.5 CAD ATDC (middle of the optimum range [23]) was used for all subsequent parametric simulations. Hence it must be remarked that no ANN was trained to calculate the Wiebe parameters in this study, unlike the model calibration method described in [19]. A summary of the main attributes of the empirical correlations is provided in Table 3. Lastly, it must be stated that the validation of these equations was not regarded as mandatory, since they were employed for very similar operating ranges to the ones shown in Table 2.

Table 3: Summary of the empirical correlations' characteristics

Involved Variable	**Calibration parameter**	**Dependent Variables**	**Equation Type**	**R^2**
EGR cooler inlet temperature	HTM of EGR line	EATS outlet temperature and EGR flow	Linear polynomial	0.75
Turbine inlet temperature	HTM of exhaust manifold	Exhaust ports temperature and exhaust gases mass flow	Linear polynomial	0.81
Exhaust line pressure drop	Discharge coef. outlet orifice	Reynolds number	Nonlinear one-variable	0.91
Torque	FMEP	Engine speed and max. cylinder pressure	Chen-Flynn model	0.81
Combustion duration	TOC1090	Engine speed, in-cylinder temperature and RGF	Linear polynomial	0.99

Once the empirical correlations were included into the model, the turbocharger was coupled and most of PI controllers were removed. Only the intake manifold pressure and temperature and the EGR rate were regulated in closed-loop configuration. In this way, the engine 1D model was ready to be used. Then, parametric 1D simulations were performed to assess the influence of the combined VVT and EGR strategies on the pumping losses, in-cylinder gas composition and heat losses. In particular, the impact on

the air management process was studied in detail by analyzing instantaneous pressures and valve mass flows in intake and exhaust manifolds. Overall, the optimization was based on finding the set of VVT settings and EGR rate which maximizes the indicated efficiency.

For that purpose, 150 cases were modeled for each steady engine operating conditions. The EGR and VVT values were varied at iso-air mass flow and iso-intake manifold temperature. In particular, six EGR rates and twenty-five pairs of VVT settings per EGR rate were considered. The maximum EGR value analyzed was 25%, given that current ignition systems allow expanding the EGR tolerance up to around 30% in gasoline engines [26]. Besides, the VNT vanes was actuated to achieve the desired AMF, if needed, and the thermal power of the EGR cooler was remained constant for all the simulations. Table 4 summarizes the main characteristics of these parametric studies for the three engine running conditions.

Finally, the VVT and EGR parameters optimized by simulation were compared with the experimental results obtained through a conventional design of experiments (DOE), which was composed of more than 300 tests, in contrast to the 25 tests used for the engine 1D model calibration (i.e., 90% less experimental work was performed by means of the methodology presented in this research study).

Table 4: Summary of the modeling parametric studies

Variable	**1500x6 study**	**2000x6 study**	**3000x12 study**
Engine speed (rpm)	1500	2000	3000
Air mass flow (kg/h)	34.5	46.5	122.5
Intake manifold temperature (ºC)	30.0	31.5	27.5
EGR (%)	0,5,10,15,20,25	0,5,10,15,20,25	0,5,10,15,20,25
VVT settings per EGR rate (points)	25	25	25
Total cases simulated	150	150	150

On the other hand, it must be noted that some non-negligible combustion aspects could not be evaluated by simulation, like the cycle-to-cycle dispersion or knocking. However, knock events were only observed for two tests at 3000 rpm and 12 bar BMEP, during the whole experimental campaign mentioned above. Despite this, the spark timing could be adjusted to set the CA50 close to the optimal range in both tests. Anyway, the settings optimized via modeling should be tested in a final experimental step to assess knocking and combustion stability, although it is out of the scope of this study. Meanwhile, it must not be forgotten that a total of 450 simulations have been run. This way, the power of the optimization method presented in this research work must be remarked, given that the required amount of potential time and resources would be much greater in the test bench.

5. Results and analysis

In this section, the results of the modeling parametric studies are presented for two of the three operating conditions: 1500 rpm and 6 bar BMEP and 3000 rpm and 12 bar BMEP. Overall, all the trends and conclusions obtained for 1500 and 2000 rpm cases are quite similar. Hence, in order not to extend the analysis, the results of the parametric study at 2000 rpm and 6 bar BMEP were excluded. Moreover, some results about the engine 1D model validation are also included. Finally, the findings achieved for 1500 and 3000 rpm parametric studies were compared with the results of a DOE process performed in the engine test rig.

5.1. 1D-Model validation

After the twenty-five engine tests were simulated to achieve fitting parameters for the model calibration, a validation process was performed before the empirical equations were defined. It must be stated that the experimental and modeling data of those same twenty-five cases (Table 2) were used for this validation stage. First, the modeled and experimental values of AMF and IMEP were compared, and an error threshold of 5% was considered for both variables to ensure the quality of the calibration procedure, as stated in the Methodology section. Figure 2 shows the values of MPE (Mean Percentage Error) in absolute value, MAPE (Mean Absolute Percentage Error) and maximum percentage error for AMF (left plot) and IMEP (right plot). Both MPE and MAPE are defined as follows:

$$\mathrm{MPE}\ (\%) = \left| 100 \cdot \frac{1}{n} \sum_{i=1}^{n} \frac{p_i - r_i}{r_i} \right| \tag{2}$$

$$\mathrm{MAPE}\ (\%) = 100 \cdot \frac{1}{n} \sum_{i=1}^{n} \left| \frac{p_i - r_i}{r_i} \right| \tag{3}$$

where 'r_i' is the experimental value, 'p_i' is the value predicted by simulation, and 'n' is the number of cases tested for each steady-state engine operating point.

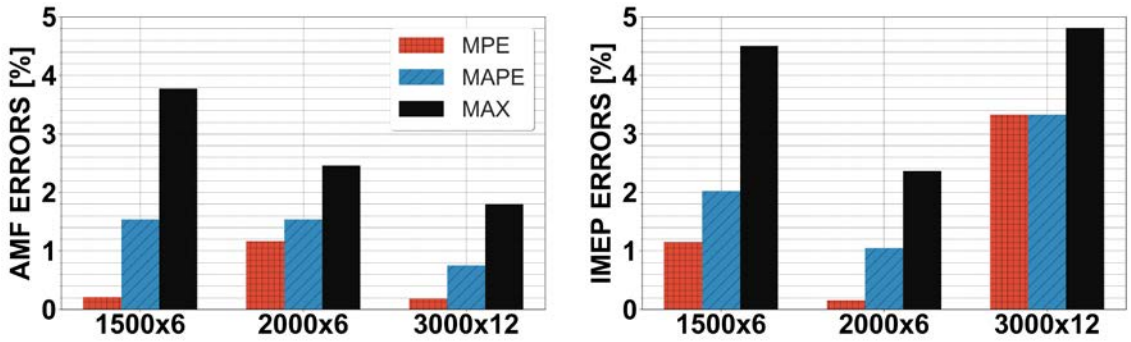

Figure 2: MPE (red), MAPE (blue) and maximum (black) errors between modeling and experimental values of AMF (left) and IMEP (right).

It must be noted that all maximum errors (shown in absolute value in Figure 2) are inside 5% threshold. In addition, it must be remarked that all MPE values are lower or close to 1%, except for IMEP at 3000 rpm and 12 bar BMEP. The latter is desirable from the point of view of the model calibration because the errors are centered around 0%. This means that additional efforts to tune fitting parameters are useless (as long as the errors are inside a limit). The rest of main cycle-averaged variables was perfectly reproduced (errors close to 0%) since the PI controllers were activated during the simulations.

Moreover, in-cylinder instantaneous pressure traces were checked for all the cases. The analysis of the parametric studies is mainly focused on the influence of combined VVT and EGR strategies on the air management process. This is because of the impact of these parameters not only on pumping losses, but also on in-cylinder gas composition and, in consequence, on heat losses. Hence a good model accuracy is desired in general but, specially, for the pumping loop, when exhaust and intake valves are open.

Figure 3 shows two in-cylinder p-V diagrams for next operating conditions: 3000 rpm and 12 bar BMEP (left) and 1500 rpm and 6 bar BMEP (right). If comparing modeling and experimental pressure traces, it can be stated that the engine model reproduces the air-management process with a remarkable accuracy, but also in-cylinder heat transfer phenomenon and the combustion process.

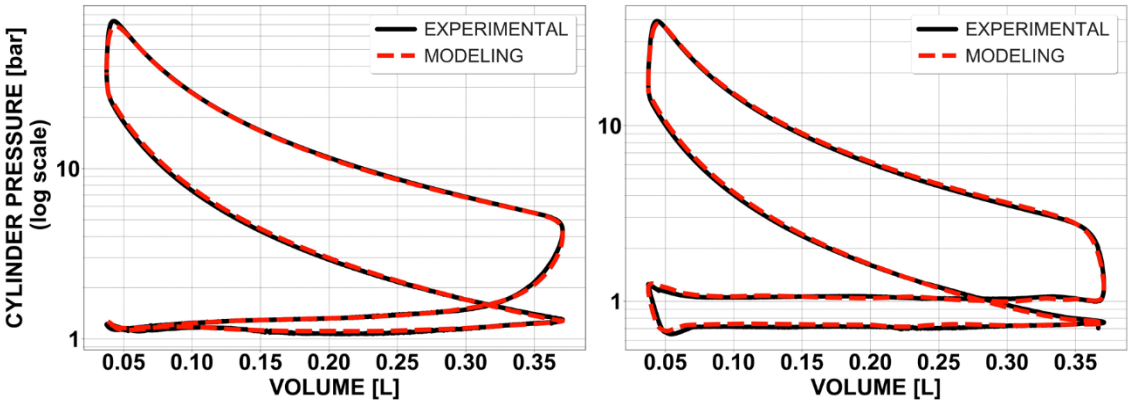

Figure 3: Experimental (black) and modeled (red) in-cylinder p-V diagrams at 3000 rpm and 12 bar BMEP (left), and at 1500 rpm and 6 bar BMEP (right).

5.2. Assessment of combined VVT, VNT and EGR strategies

5.2.1. 1500-rpm parametric study

A parametric study was done via modeling at 1500 rpm and 6 bar BMEP. The EGR rate was varied from 0 to 25%. Regarding the VVT system, twenty-five pairs of IVO (intake valve opening) and EVC (exhaust valve closing) values were simulated for each EGR rate (from minimum to maximum valve overlap). The VNT vanes were kept open for all the simulations, given that the iso-AMF condition could be achieved without the need of boosting. The ambient conditions (1 bar and 25 ºC) and a value of air-to-fuel ratio (AFR) equal to 1 were imposed in the engine model as well.

After a total of 150 simulations, contour maps of pumping losses, in-cylinder residual gas fraction (RGF), heat losses and indicated efficiency were obtained for each EGR rate, as functions of IVO (X-axis) and EVC (Y-axis). Figure 4 shows these contour plots for 10% EGR. The pumping losses are defined as the area of the pumping loop divided by cylinder volume, while the residual gas fraction is calculated as the ratio between in-cylinder mass of burned gases (including external EGR) and total in-cylinder mass at the combustion start. Besides, the heat losses attached are referred to the cycle-averaged in-cylinder heat transfer. It must be also reminded that the VVT system enables to advance IVO and delay EVC up to forty degrees. This way, the values of IVO and EVC equal to 0-0 and 40-40 provide minimum and maximum valve overlaps, respectively.

A pumping losses reduction and an in-cylinder RGF increase are observed in Figure 4 when the valve overlap is enlarged. This is because the difference between intake and exhaust manifold pressures at IVO timing produces back flows in intake valves. Hence a lower throttling is required to remain constant the air mass flow, and so pumping losses are minimized for a large overlap period. The mentioned back flows in intake valves can be noticed in Figure 5, where the instantaneous mass flows in intake and exhaust valves (top) and pressure traces (bottom) are provided for 10% EGR, with minimum (VVT 0-0) and maximum (VVT 40-40) valve overlap. It must be also noted that a negative intake valve flow means that gases are leaving the cylinder towards intake ports. Meanwhile, a negative exhaust valve flow denotes that gases are entering the cylinder from exhaust ports.

Regarding heat losses, its minimum value for 10% EGR was obtained by fully advancing IVO and partially delaying EVC, as shown in Figure 4. A priori, an in-cylinder RGF increase generates a heat losses reduction, due to a lower combustion temperature. However, this tendency is not exactly observed if comparing heat losses and RGF surfaces (Figure 4), given that an RGF increase also results in higher in-cylinder temperature values during the intake and compression strokes. Furthermore, the indicated efficiency maximum is also achieved for a large overlap period, due to the combination of lower pumping and heat losses.

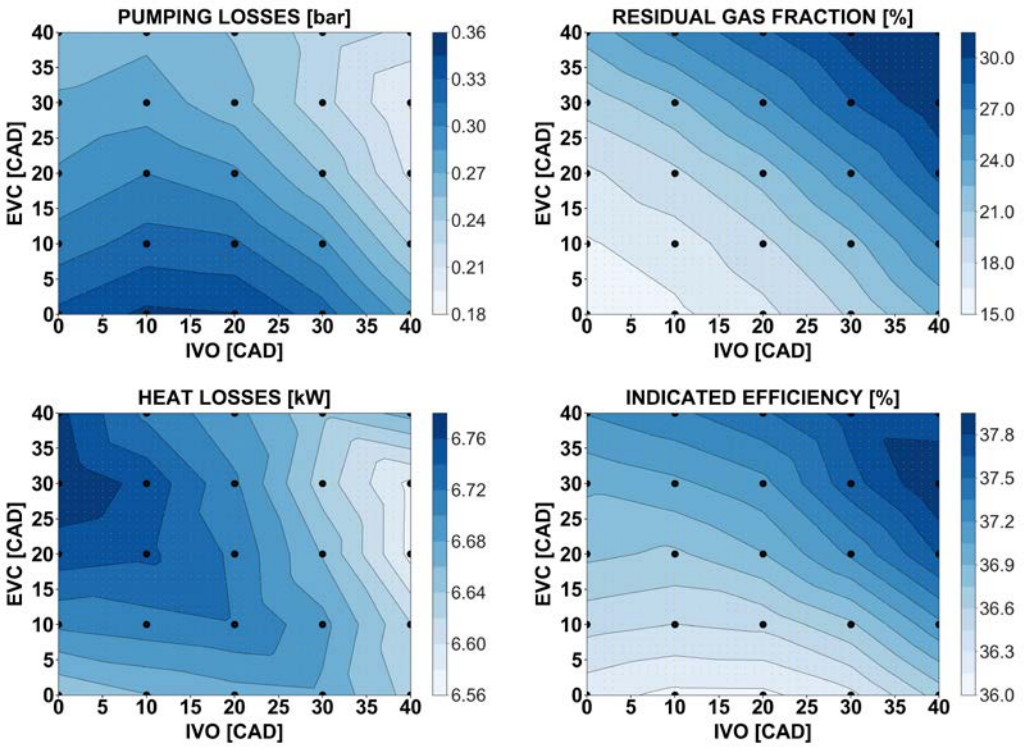

Figure 4: Contour maps of modeled pumping losses (top left), in-cylinder RGF (top right), heat losses (bottom left) and indicated efficiency (bottom right), as functions of IVO and EVC, for 10% EGR at 1500 rpm and 6 bar BMEP. Black dots represent all VVT configurations modeled.

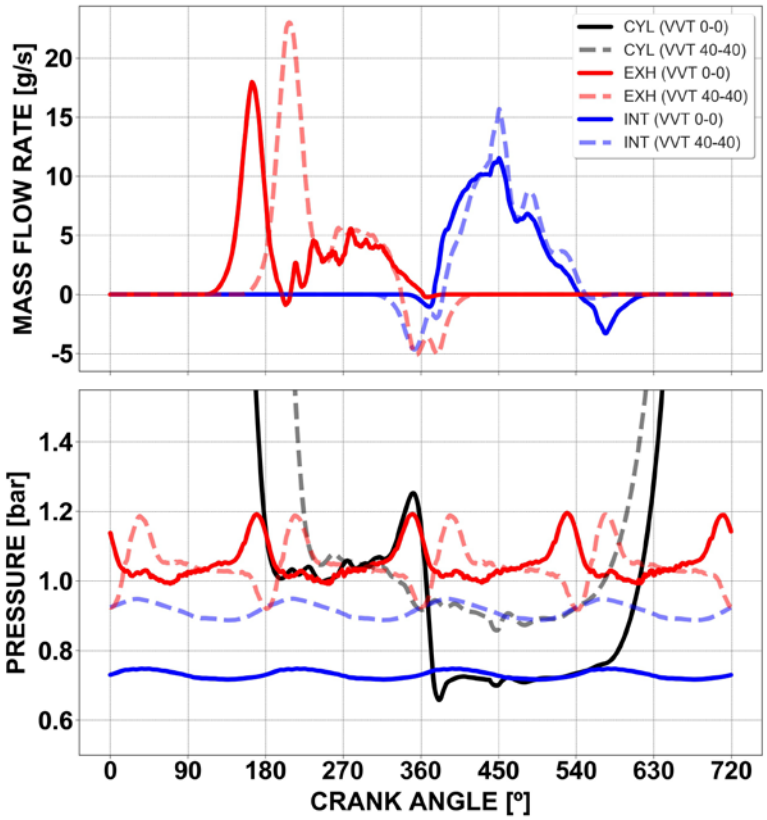

Figure 5: Modeled instantaneous valve mass flow (top) and pressure (bottom) in cylinder (CYL), intake manifold (INT) and exhaust manifold (EXH) for 10% EGR at 1500 rpm and 6 bar BMEP, and for minimum (VVT 0-0) and maximum (VVT 40-40) overlaps.

Figure 6 shows the variation of pumping losses (represented by the pumping mean effective pressure [PMEP]), in-cylinder RGF, heat losses (HL) and indicated efficiency (IE) for different EGR rates, for the minimum (cross markers) and maximum (circle markers) overlap. In this figure, it can be noticed that the EGR addition reduces pumping losses, because a higher intake manifold pressure is needed to keep the iso-air mass flow condition. However, the EGR effect on pumping losses is smaller for the maximum overlap. It can be explained through instantaneous mass flows in intake and exhaust valves and pressure traces, which are provided in Figure 7 for different EGR rates (the whole engine cycle is not shown, but a zoom around BDC). At IVO timing, the back flows in intake valves for the maximum overlap are slightly lowered when EGR rate is increased (top plot in Figure 7). Therefore, these different backflow levels cause that the pressure increment required in the intake manifold is not proportional to the EGR addition and, in consequence, pumping losses reduction is less steep with the maximum valve overlap (Figure 6).

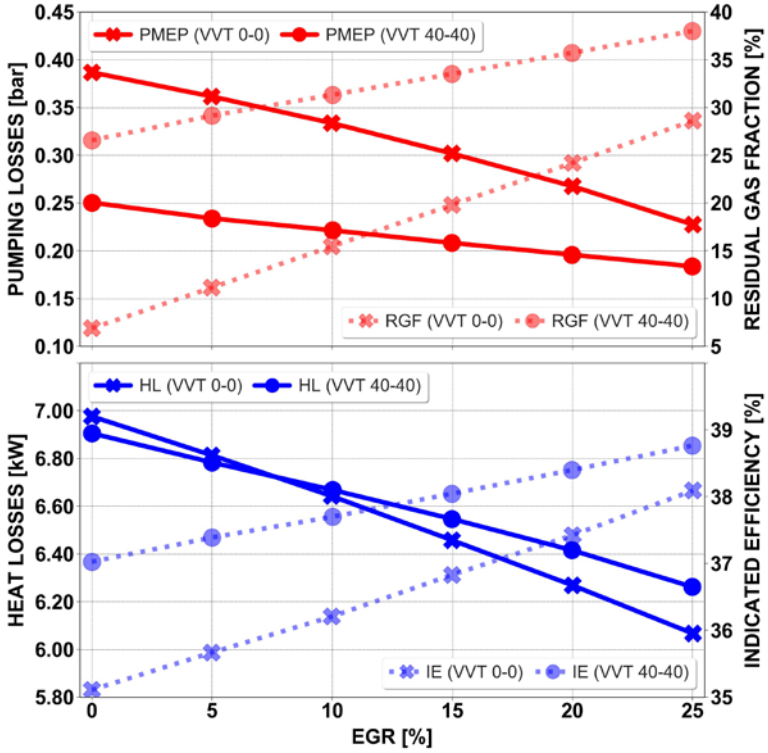

Figure 6: Evolution of modeled pumping losses (PMEP), in-cylinder RGF, heat losses (HL) and indicated efficiency (IE) for different EGR rates at 1500 rpm and 6 bar BMEP, and for minimum (VVT 0-0) and maximum (VVT 40-40) overlap.

The EGR dilution effect also leads to a decrease in heat losses, because of lower in-cylinder temperature values during the combustion and exhaust strokes. Hence the indicated efficiency maximum was achieved with 25% EGR and a large overlap period, due to combined pumping and heat losses reduction. A 3.5% indicated efficiency improvement was observed if comparing the best and worst configuration of EGR and VVT systems (Figure 6). Besides, it must be remarked that the VVT impact on indicated efficiency is less relevant as EGR is increased (Figure 6). This is caused by a smaller EGR effect on pumping losses for the maximum overlap, as said above, along with lower

heat losses for the minimum overlap from 10% EGR. Therefore, it can be assumed that VVT is not especially critical for high EGR rates, given that a difference in indicated efficiency of around 0.5% between the minimum and maximum valve overlap was just noticed.

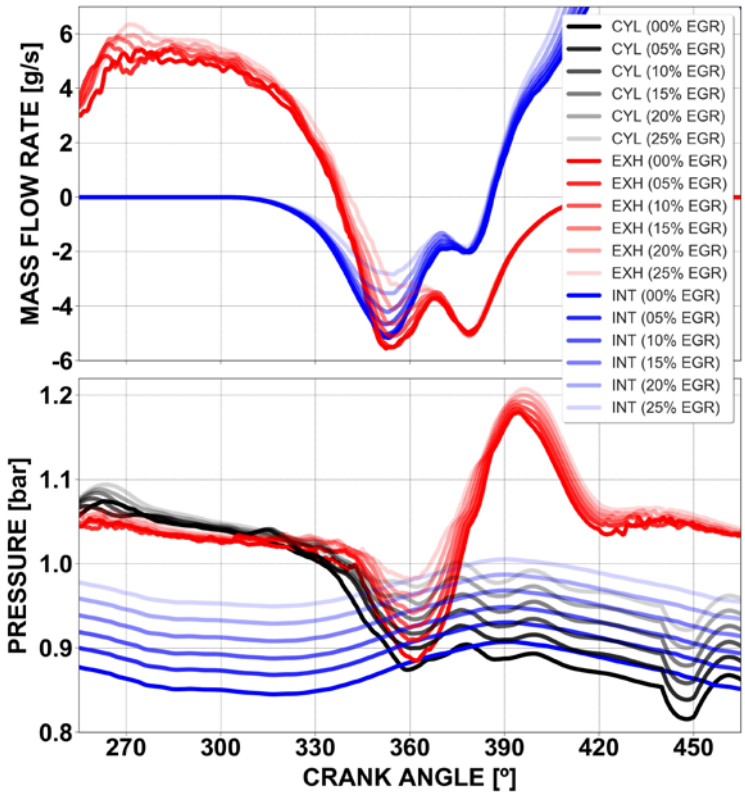

Figure 7: Modeled instantaneous valve mass flow (top) and pressure (bottom) in cylinder (CYL), intake manifold (INT) and exhaust manifold (EXH) for different EGR rates at 1500 rpm and 6 bar BMEP, and for maximum overlap (VVT 40-40).

5.2.2. 3000-rpm parametric study

A second parametric study was performed via modeling at 3000 rpm and 12 bar BMEP, by following the same procedure. Again, the EGR rate was modified in a range from 0 to 25%, and twenty-five pairs of VVT (IVO and EVC) settings were simulated for each EGR rate. Besides, the VNT vanes were partially closed for EGR rates higher than 15% to reach the desired AMF. The ambient conditions (1 bar and 25 ºC) and a value of air-to-fuel ratio (AFR) equal to 1 were imposed in the engine model as well. Once more, contour maps of pumping losses, in-cylinder RGF, heat losses and indicated efficiency were obtained for each EGR rate, as functions of IVO and EVC. Figure 8 shows these contour plots for 20% EGR. In addition, Figure 9 illustrates the instantaneous mass flows in intake and exhaust valves (top) and pressure traces (bottom) also for 20% EGR and for three VVT configurations: 0-0 (IVO-EVC), 0-40 and 40-40.

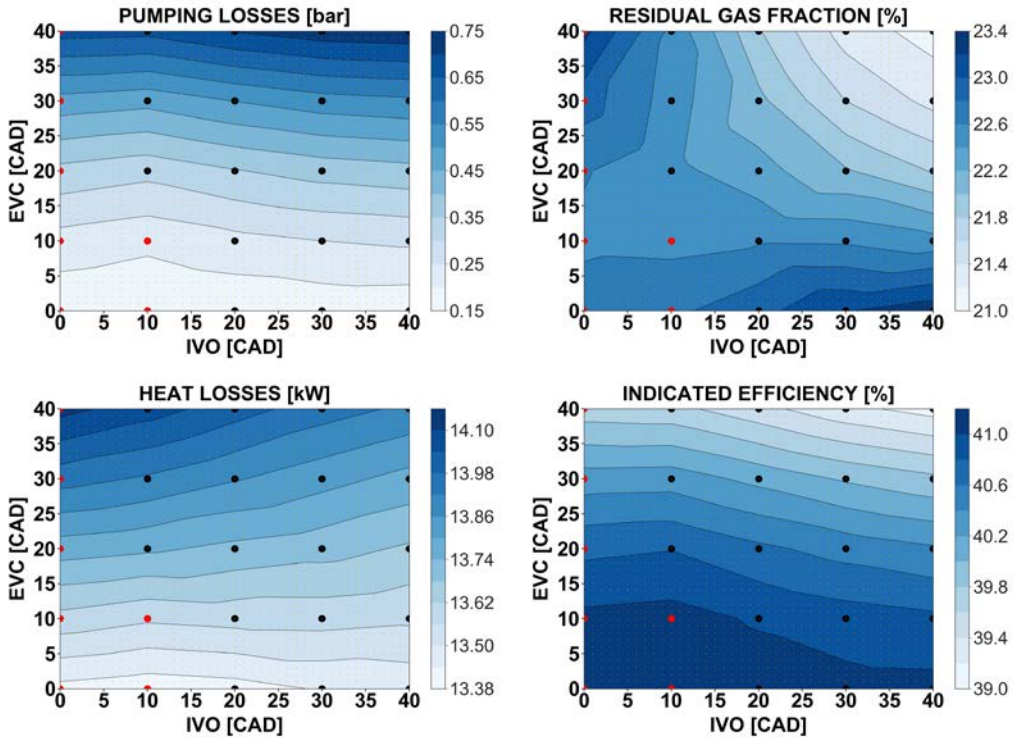

Figure 8: Contour maps of modeled pumping losses (top left), in-cylinder RGF (top right), heat losses (bottom left) and indicated efficiency (bottom right), as functions of IVO and EVC, for 20% EGR at 3000 rpm and 12 bar BMEP. All VVT configurations are represented with red (VNT vanes partially closed) and black (vanes fully open) dots.

At first sight, it can be noted that the pumping losses were minimized by fully advancing EVC (equal to zero) and the impact of IVO on PMEP can be neglected (Figure 8). If comparing the 0-0 and 0-40 cases, the differences of mean pressure between the exhaust and intake manifolds are quite similar for both VVT configurations (Figure 9). However, the pumping losses are much higher for the 0-40 case, since a delay of 40 CAD in EVC produces an in-cylinder pressure increase around BDC (270 CAD), and so the pumping loop is enlarged. The latter can be noticed in Figure 10, where the p-V diagrams for 20% EGR and three VVT configurations (0-0, 0-40 and 40-40) are attached. Hence it can be concluded that the difference of mean pressure between both manifolds is not always a reliable indicator to estimate pumping losses.

Moreover, all VVT configurations simulated for each EGR rate were represented with dots of two colors in Figure 8, depending on whether VNT vanes were partially closed (red) or fully open (black). It was required to actuate on VNT vanes when IVO was not higher than 10. This is because intake manifold pressure had to be increased for IVO values close to zero, in order to compensate the back flows observed just before intake valve closing (top plot in Figure 9). Regarding heat losses, its minimum for 20% EGR was also obtained by fully advancing EVC (Figure 8), due to a lower in-cylinder gas temperature during the exhaust stroke. Therefore, the indicated efficiency maximum was also achieved in the same way, given that both pumping work and heat losses are reduced as EVC timing is advanced. Besides, it must be noted that the effect of IVO on heat losses and indicated efficiency is also marginal.

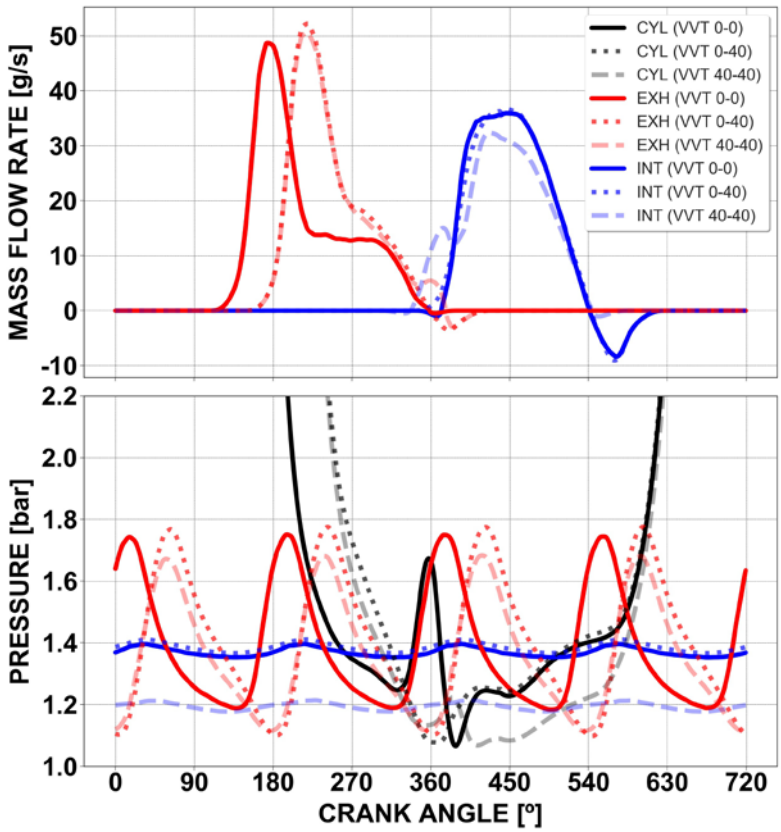

Figure 9: Modeled instantaneous valve mass flow (top) and pressure (bottom) in cylinder (CYL), intake manifold (INT) and exhaust manifold (EXH) for 20% EGR at 3000 rpm and 12 bar BMEP, and for the 0-0 (IVO-EVC), 0-40 and 40-40 VVT configurations.

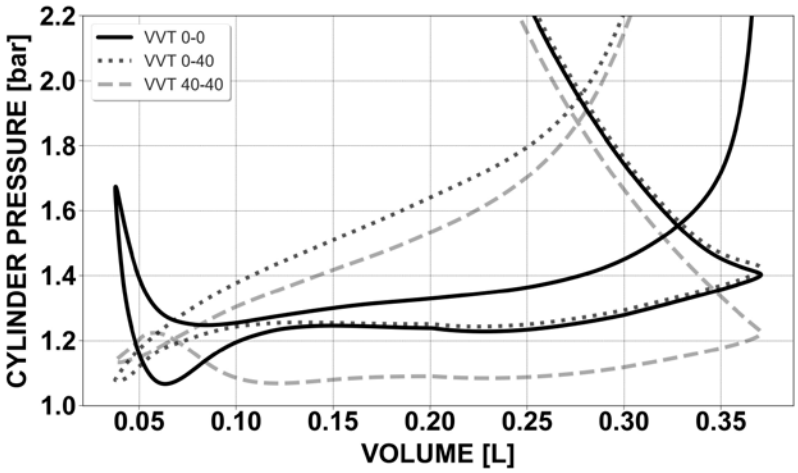

Figure 10: Modeled p-V diagrams for 20% EGR at 3000 rpm and 12 bar BMEP, and for the 0-0 (IVO-EVC), 0-40 and 40-40 VVT configurations.

Figure 11 shows the evolution of pumping losses (PMEP), in-cylinder RGF, heat losses (HL), indicated efficiency (IE), compressor efficiency (CE), turbine efficiency (TE), intake manifold pressure (IMP) and exhaust manifold pressure (EMP), for different EGR rates and the 0-0 (IVO-EVC) and 0-40 VVT configurations. In addition, Figure 12 presents two p-V diagrams also for different EGR rates and the same VVT settings. Focusing on pumping losses, two different trends were observed depending on VVT

configuration. On one side, no variations in PMEP were obtained with EGR rates up to 15% for VVT settings equal to 0-40 (circle markers in Figure 11). Delaying EVC without advancing IVO moves the intersection point that divides the work and pumping loops away from BDC (bottom plot in Figure 12). For that reason, pumping losses were not lowered when EGR rate was increased, although the difference of mean pressure between both manifolds was reduced (bottom-right plot in Figure 11); given that the intake pressure increment also leads to a pumping loop enlargement between BDC and the above-mentioned intersection point (bottom plot in Figure 12). Meanwhile, the throttle valve was fully open for EGR rates higher than 15%, and so the AMF was controlled by means of the VNT position. Despite a turbine efficiency increment, pumping losses were slightly increased from 15% EGR.

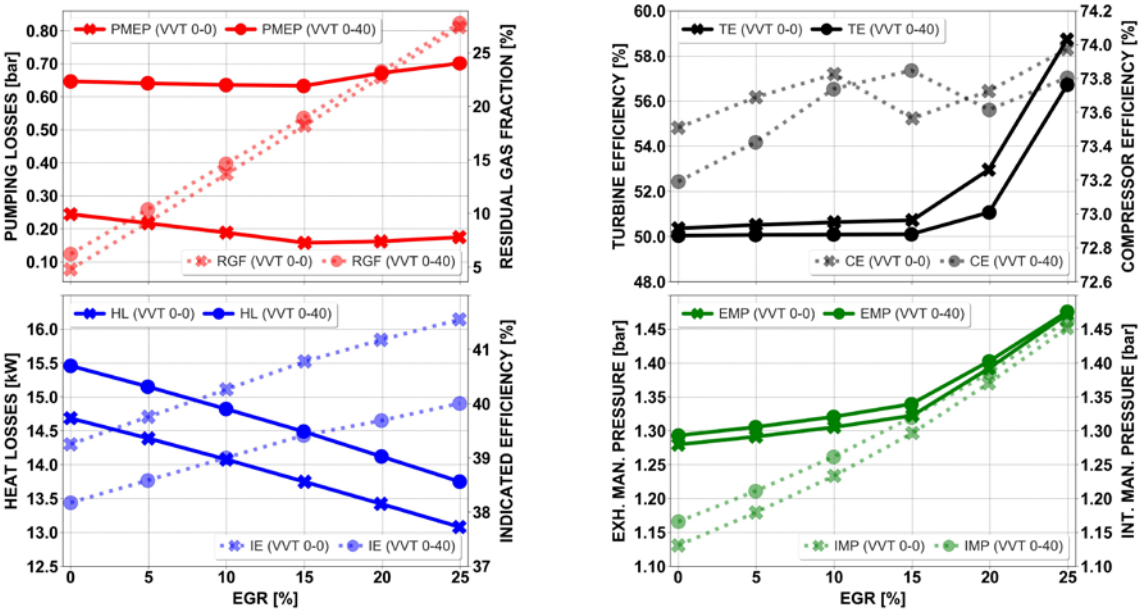

Figure 11: Evolution of modeled pumping losses (PMEP), in-cylinder RGF, heat losses (HL), indicated efficiency (IE), compressor efficiency (CE), turbine efficiency (TE), intake manifold pressure (IMP) and exhaust manifold pressure (EMP) for different EGR rates at 3000 rpm and 12 bar BMEP, and for the 0-0 (IVO-EVC) and 0-40 VVT configurations.

On the other side, pumping losses were decreased with EGR rates up to 15% and minimum valve overlap (cross markers in Figure 11), due to a higher intake manifold pressure required to reach the same air mass flow (bottom-right plot in Figure 11). In this case, that pressure increment results in a narrowing of the pumping loop, as seen in the top plot in Figure 12. In addition, PMEP was kept almost constant for EGR rates higher than 15%. This is because the VNT vanes closure did not produce a sharp increase of exhaust manifold pressure, mainly thanks to around 8% turbine efficiency increment from 15 to 25% EGR (top-right plot in Figure 11).

The addition of EGR also resulted in a reduction in heat losses, due to a lower in-cylinder temperature values during the combustion and exhaust strokes. Hence the indicated efficiency was optimized with 25% EGR and an EVC equal to zero, as a consequence of minimizing pumping and heat losses. An improvement in indicated efficiency of 3.4%

was observed if comparing the best and worst configuration of EGR and VVT systems (Figure 11). Besides, it must be stated that the VVT effect on engine performance is remarkable in this case, given that the indicated efficiency was increased by around 1.5% when EVC was fully advanced (equal to 0) with 25% EGR (Figure 11). Finally, it must be also mentioned that the VNT technology enables to operate with EGR rates higher than 15%, without a pumping losses penalization. Therefore, the VNT led to a 0.8% indicated efficiency improvement when EGR was enlarged from 15 to 25% with the minimum valve overlap (Figure 11).

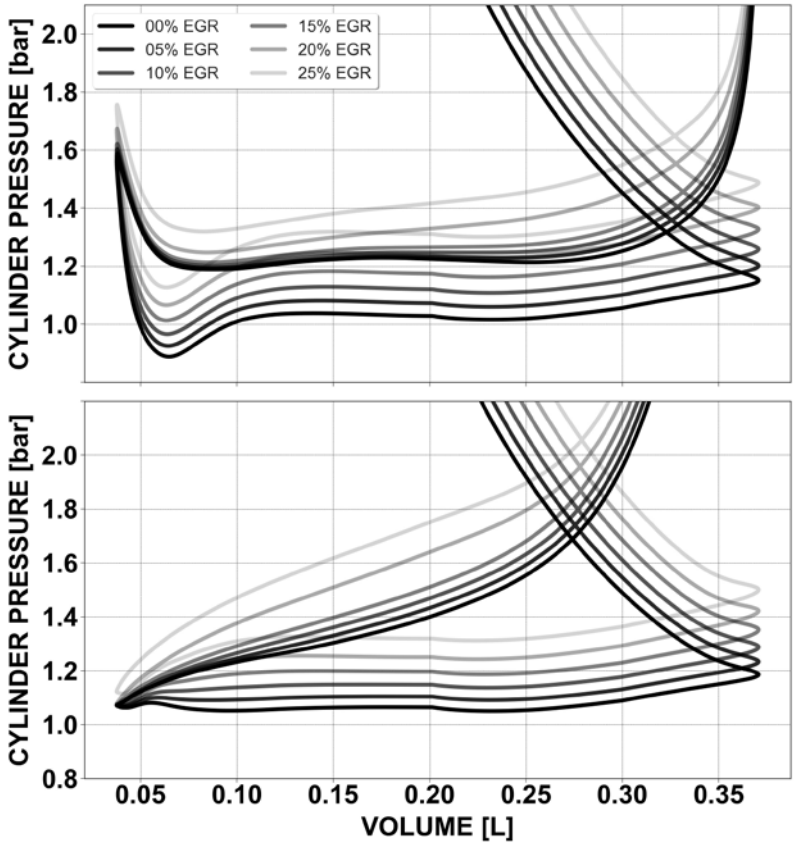

Figure 12: Modeled p-V diagrams for different EGR rates at 3000 rpm and 12 bar BMEP, and for VVT settings (IVO-EVC) equal to 0-0 (top) and 0-40 (bottom).

5.3. Experimental validation

After the parametric studies, modeling results were compared with experimental data from a DOE carried out in the engine test bench to minimize fuel consumption. The DOE procedure was composed of two stages in which more than 300 experiments were completed. In a first step, 100 tests were performed for each operating point by varying four parameters: IVO angle, EVC angle, EGR rate and spark timing. If needed, the VNT vanes were also actuated to reach the desired load. In a final step, the best combinations of IVO, EVC and EGR were again tested, but now the spark timing was adjusted in real time to set the CA50 inside the optimum range [23] for each test. Moreover, it must be stated that the experiments with an IMEP coefficient of variation (COV) higher than 3% were not accepted for the optimization of engine fuel efficiency.

Table 5 shows the main parameters of the three best experimental cases in terms of fuel consumption, for two steady engine running conditions: 1500 rpm and 6 bar BMEP and 3000 rpm and 12 bar BMEP. Moreover, Table 6 presents the optimized VVT and EGR values achieved by simulation, also for the same two operating conditions. Regarding the VNT values shown in both tables, a percentage of 100 means the vanes are fully open. Starting with the point of 3000 rpm, experimental and modeling results are quite similar. The optimum EVC obtained by simulation is very close to the optimal experimental range (Table 5 and Table 6). It must be reminded that the IVO impact on indicated efficiency could be neglected (bottom-right plot in Figure 8), so the differences in IVO should not be relevant in this case. In addition, the optimum experimental EGR rate (25%) matches the maximum EGR modeled. An EGR tolerance of 30.9% was found via experimental. The VNT position is around 60% in both experimental and modeling cases. Finally, it must be specially remarked that the model prediction in terms of pumping losses, indicated efficiency and fuel consumption is notable (Table 5 and Table 6).

Table 5: Best DOE results obtained via experimental

Case	IVO (-)	EVC (-)	EGR (%)	VNT (%)	BSFC (g/kWh)	η_{ind} (%)	PMEP (bar)
1500x6	0	0	28.4	100	248.7	37.6	0.18
1500x6	33	28	20.4	100	250.0	37.4	0.19
1500x6	0	0	25.4	100	251.2	37.3	0.23
3000x12	18	2	25.5	59	223.0	41.3	0.22
3000x12	20	1.5	25.5	59	223.1	41.3	0.22
3000x12	13	4	25.5	59	223.6	41.2	0.25

Table 6: Best parametric studies results obtained via modeling

Case	IVO (-)	EVC (-)	EGR (%)	VNT (%)	BSFC (g/kWh)	η_{ind} (%)	PMEP (bar)
1500x6	35	30	25	100	240	39.0	0.15
3000x12	5	0	25	64	222	41.5	0.20

Regarding the point of 1500 rpm, some similarities between DOE data and modeling results were also found, but the matching was not perfect. Firstly, the experimental values of indicated efficiency for 20.4% and 25.4% EGR are almost identical (Table 5), and their corresponding VVT settings (IVO-EVC) are 33-28 and 0-0, respectively. The same trend was observed by simulation, given that the following two cases in Figure 6 have quite similar indicated efficiency values: 25% EGR and minimum overlap (0-0) and 20% EGR and maximum overlap (40-40). Moreover, the experimental VVT settings for 20.4% EGR are located inside the predicted optimum VVT range for 20% EGR. Figure 13 presents the contour map of modeled indicated efficiency as a function of IVO and EVC, at 1500 rpm and 6 bar BMEP with 20% EGR.

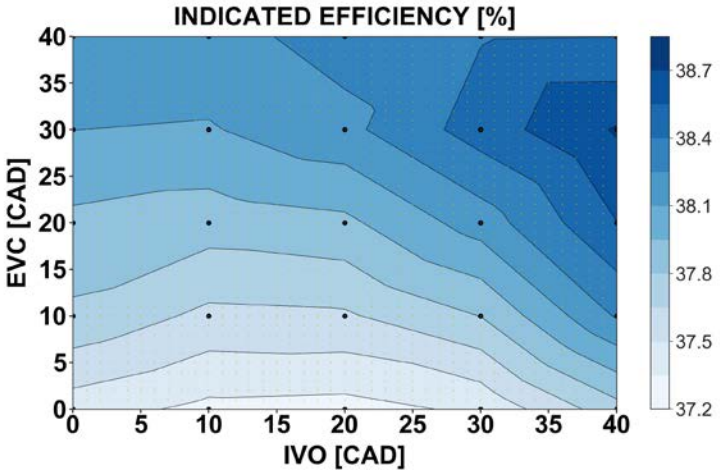

Figure 13: Contour map of modeled indicated efficiency as a function of IVO and EVC, at 1500 rpm and 6 bar BMEP with 20% EGR.

In contrast, it must be stated that the optimum VVT settings (0-0) found via DOE for 25% EGR do not match the values achieved via modeling. An experimental combustion deterioration for large overlap periods which cannot be captured by the model is the explanation to this matter. An additional experimental work was performed to verify this behavior. Two EGR sweeps were tested at 1500 rpm and 6 bar BMEP for maximum and minimum valve overlap. Again, the spark timing was adjusted in real time to set the CA50 inside the optimum range [23] for each test, and the IMEP coefficient of variation was also estimated.

Figure 14 shows the IMEP COV values for both experimental EGR sweeps. The COV was suddenly increased from around 20% EGR with maximum overlap (40-40), due to an excessive in-cylinder residual gas fraction. However, this sharp change was not observed with minimum overlap (0-0) until around 28% (Figure 14). Hence it can be concluded that minimizing valve overlap at 1500 rpm and 6 bar BMEP allows expanding EGR tolerance, and so reducing pumping and heat losses more without causing combustion instabilities. In consequence, the engine fuel consumption was minimized via DOE with 28.4% EGR and minimum overlap (Table 5).

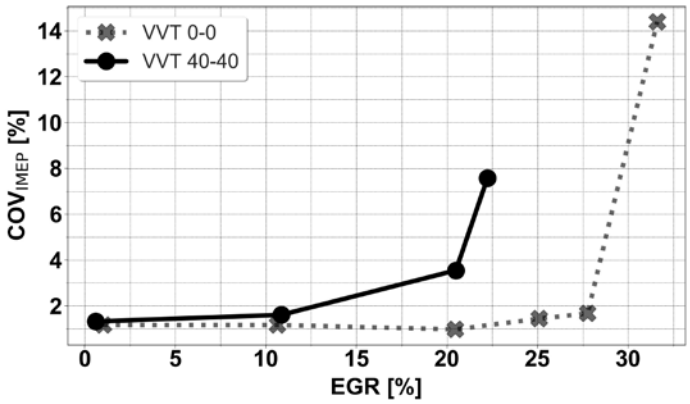

Figure 14: Evolution of experimental IMEP coefficient of variation for different EGR rates at 1500 rpm and 6 bar BMEP, for minimum (VVT 0-0) and maximum (VVT 40-40) valve overlap.

6. Conclusions

An engine 1D model was calibrated by using the data from 25 experiments, and then a total of 150 simulations per operating point were performed to optimize VVT settings and EGR rate. The results of these simulations were widely evaluated in terms of pumping losses, in-cylinder residual gas composition, heat losses and indicated efficiency. A deep analysis of instantaneous pressure traces and mass flows in intake and exhaust valves was given too. Finally, modeling results were also compared with the experimental data obtained through a DOE process, with more than 300 tests in total. Thanks to the similitude between modeling and experimental performances, it must be remarked that the methodology used in the present work allows obtaining reliable findings with a 90% workload reduction in the engine test bench.

At 1500 rpm and 6 bar BMEP, a 3.5% indicated efficiency improvement was observed by simulation if comparing the best and worst configuration of EGR and VVT systems. The indicated efficiency was maximized by simulation with 25% EGR rate, while fuel consumption was minimized via DOE with 28.4% EGR rate. Although the impact of VVT configuration on indicated efficiency could seem marginal for high EGR rates in this case, a proper VVT adjustment was experimentally required to increase EGR rate without combustion instabilities. Despite the matching between modeling and DOE results was not perfect, significant similarities were found.

At 3000 rpm and 12 bar BMEP, based on simulation results, the indicated efficiency was increased by 3.4% when the best and worst combinations of EGR rate and VVT settings were compared. The maximum indicated efficiency was found by simulation with 25% EGR and a short overlap period. Advancing fully EVC led to a reduction in pumping and heat losses, while the impact of IVO could be neglected. Besides, the VNT turbocharger allowed increasing EGR rate from 15% to 25% without a penalization in PMEP, thus improving the indicated efficiency by an additional 0.8%. The same trends were observed via DOE.

Finally, it must be stated that combustion instabilities were observed in the experimental tests at 1500 rpm and 6 bar BMEP, especially for high in-cylinder residual gas fraction. Knock events also appeared at 3000 rpm and 12 bar BMEP. Both phenomena cannot be replicated by the model. Therefore, the VVT and EGR values optimized via modeling should be tested in a final experimental step to assess these matters.

References

1. Lumsden, G., OudeNijeweme, D., Fraser, N., Blaxill, H., "Development of a Turbocharged Direct Injection Downsizing Demonstrator Engine", SAE Int. J. Engines, vol. 2, pp. 1420-1432, 2009. 10.4271/2009-01-1503

2. Fraser, N., Blaxill, H., Lumsden, G., Bassett, M., "Challenges for Increased Efficiency through Gasoline Engine Downsizing", SAE Int. J. Engines, vol. 2, pp. 991-1008, 2009. 10.4271/2009-01-1053

3. Shahed, S., Bauer, K., "Parametric Studies of the Impact of Turbocharging on Gasoline Engine Downsizing", SAE Int. J. Engines, vol. 2, pp. 1347-1358, 2009. 10.4271/2009-01-1472

4. Coltman, D., Turner, J. W. G., Curtis, R., Blake, D., Holland, B., Pearson R. J., Arden, A., Nuglisch, H., "Project Sabre: A Close-Spaced Direct Injection 3-Cylinder Engine with Synergistic Technologies to Achieve Low CO2 Output", SAE Int. J. Engines, vol. 1, pp. 129-146, 2009. 10.4271/2008-01-0138

5. He, Y., Liu, J., Zhu, B., Sun, D., "Development of a Miller cycle engine with single-stage boosting and cooled external exhaust gas recirculation", Proceedings of the Institution of Mechanical Engineers, Part D: Journal of Automobile Engineering, vol. 231, pp. 766-780, 2017. 10.1177/0954407016662567

6. Zhang, S., Li, C., Liu, R., Bao, J., Chi, M., "Effects of the variable valve lift difference on in-cylinder gas flow in a four-valve gasoline engine", Proceedings of the Institution of Mechanical Engineers, Part D: Journal of Automobile Engineering, vol. 233, pp. 1806-1817, 2019. 10.1177/0954407018789321

7. McGhee, M., Wang, Z., Bech, A., Shayler, P. J., Witt, D., "The effects of cylinder deactivation on the thermal behaviour and fuel economy of a three-cylinder direct injection spark ignition gasoline engine", Proceedings of the Institution of Mechanical Engineers, Part D: Journal of Automobile Engineering, vol. 233, pp. 2838-2849, 2019. 10.1177/0954407018806744

8. Golzari, R., Zhao, H., Hall, J., Bassett, M., Williams, J., Pearson, R., "Impact of intake port injection of water on boosted downsized gasoline direct injection engine combustion, efficiency and emissions", International Journal of Engine Research, 2019. 10.1177/1468087419832791

9. Potteau, S., Lutz, P., Leroux, S., Moroz, S., Tomas, E., "Cooled EGR for a Turbo SI Engine to Reduce Knocking and Fuel Consumption", SAE Technical Paper 2007-01-3978, 2007. 10.4271/2007-01-3978

10. Kumano, K., Yamaoka, S., "Analysis of Knocking Suppression Effect of Cooled EGR in Turbo-Charged Gasoline Engine", SAE Technical Paper 2014-01-1217, 2014. 10.4271/2014-01-1217

11. Siokos, K., Koli, R., Prucka, R., Schwanke, J., Miersch, J., "Assessment of Cooled Low Pressure EGR in a Turbocharged Direct Injection Gasoline Engine", SAE Int. J. Engines, vol. 8, pp. 1535-1543, 2015. 10.4271/2015-01-1253

12. Parsons, D., Akehurst, S., Brace, C., "The potential of catalysed exhaust gas recirculation to improve high-load operation in spark ignition engines", International Journal of Engine Research, 2015. 10.1177/1468087414554628

13. Alger, T., Chauvet, T., Dimitrova, Z., "Synergies between High EGR Operation and GDI Systems", SAE Int. J. Engines, vol. 1, pp. 101-114, 2009. 10.4271/2008-01-0134

14. Luján, J. M., Climent, H., Novella, R., Rivas-Perea, M. E., "Influence of a low pressure EGR loop on a gasoline turbocharged direct injection engine", Applied Thermal Engineering, 2015. 10.1016/j.applthermaleng.2015.06.039

15. Torregrosa, A. J., Galindo, J., Guardiola, C., Varnier O., "Combined experimental and modeling methodology for intake line evaluation in turbocharged diesel engines", Int. J. Automot. Technol., vol 12, pp. 359-367, 2011. 10.1007/s12239-011-0042-8

16. Faghani, E., Andric, J., Sjoblom, J., "Toward an Effective Virtual Powertrain Calibration System", SAE Technical Paper 2018-01-0007, 2018. 10.4271/2018-01-0007

17. Albrecht, A., Corde, G., Knop, V., Boie, H., Castagne, M., "1D Simulation of Turbocharged Gasoline Direct Injection Engine for Transient Strategy Optimization", SAE Technical Paper 2005-01-0693, 2005. 10.4271/2005-01-0693

18. Payri, F., Benajes, J., Galindo, J., Serrano, J. R., "Modelling of turbocharged diesel engines in transient operation. Part 2: Wave action models for calculating the transient operation in a high speed direct injection engine", Proceedings of the Institution of Mechanical Engineers, Part D: Journal of Automobile Engineering, vol. 216, pp. 479-493, 2002. 10.1243/09544070260137507

19. Serrano, J., Climent, H., Navarro, R., González-Domínguez, D., "Methodology to Standardize and Improve the Calibration Process of a 1D Model of a GTDI Engine", SAE Technical Paper 2020-01-1008, 2020. 10.4271/2020-01-1008

20. Payri, F., Lujan, J., Climent, H., Pla, B., "Effects of the Intake Charge Distribution in HSDI Engines", SAE Technical Paper 2010-01-1119, 2010. 10.4271/2010-01-1119

21. Pla, B., De La Morena, J., Bares, P., Jiménez, I., "Knock Analysis in the Crank Angle Domain for Low-Knocking Cycles Detection", SAE Technical Paper 2020-01-0549, 2020. 10.4271/2020-01-0549

22. Pla, B., De la Morena, J., Bares, P., Jiménez, I., "Cycle-to-cycle combustion variability modelling in spark ignited engines for control purposes", International Journal of Engine Research, 2020. 10.1177/1468087419885754

23. Lavoie, G. A., Ortiz-Soto, E., Babajimopoulos, A., Martz, J. B., Assanis, D. N., "Thermodynamic sweet spot for high-efficiency, dilute, boosted gasoline engines", International Journal of Engine Research, 2013. 10.1177/1468087412455372

24. Ghojel, J. I., "Review of the development and applications of the Wiebe function: A tribute to the contribution of Ivan Wiebe to engine research", International Journal of Engine Research, 2010. 10.1243/14680874JER06510

25. Galindo, J., Climent, H., Plá, B., Jiménez, V. D., "Correlations for Wiebe function parameters for combustion simulation in two-stroke small engines", Applied thermal engineering, vol. 31, pp. 1190-1199, 2011. 10.1016/j.applthermaleng.2010.12.020

26. Shimura, R., Zhao, H., Wang, X., "Expansion of external EGR effective region and influence of dilution on boosted operation of a downsized turbocharged GDI engine", SAE Technical Paper 2019-01-2252, 2019. 10.4271/2019-01-2252